Supplementary Information

An environment-friendly and acid-degradable polymer templated synthesis of single-crystalline hierarchical zeolites

Yuan Hu,[a] Yuan-Yuan Yue,*[a, b] Chan Wang,[a, b] Hai-Bo Zhu,[a, b] S. Ted Oyama,[a] Xiao-Jun Bao*[b, c]

[a]National Engineering Research Center of Chemical Fertilizer Catalyst, College of Chemical Engineering, Fuzhou University, Fuzhou 350116, P. R. China.

[b]Qingyuan Innovation Laboratory, Quanzhou 362801, P. R. China.

[c]State Key Laboratory of Photocatalysis on Energy & Environment, College of Chemistry, Fuzhou University, Fuzhou 350116, P. R. China.

*Corresponding authors. E-mails: yueyy@fzu.edu.cn (Y. Yue) and baoxj@fzu.edu.cn (X. Bao).

The content of ESI

Supplementary Figures

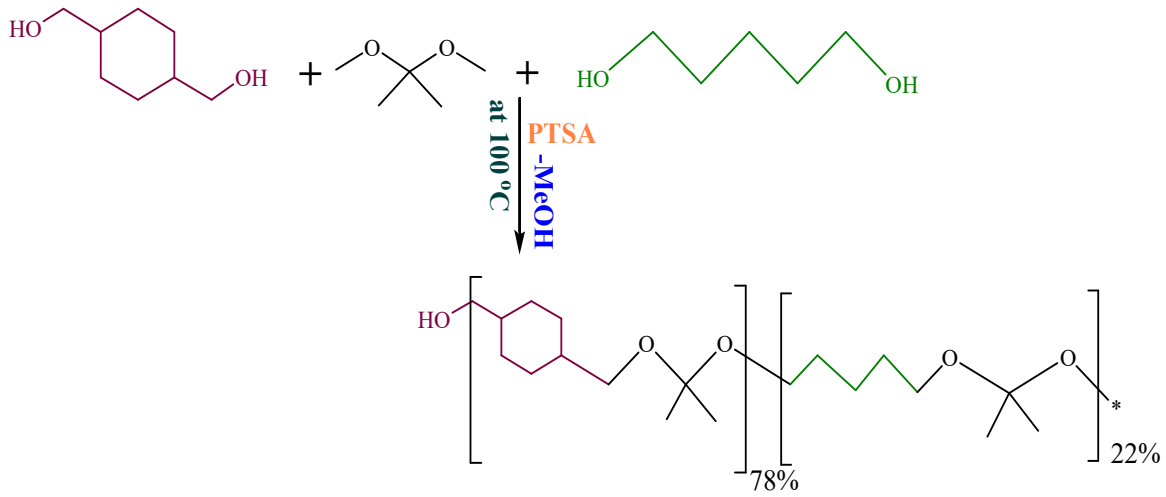

Fig. S1 Reaction formula for synthesizing PK3. This polymer was synthesized via a step-growth polymerization reaction, which is achieved through a ketal exchange reaction between two diols (1,4-cyclohexanedimethanol and 1,5-pentanediol) and 2,2-dimethoxypropane with p-toluenesulfonic acid as the catalyst. The reaction product was purified by precipitation in hexane to remove the catalyst and unreacted monomers.

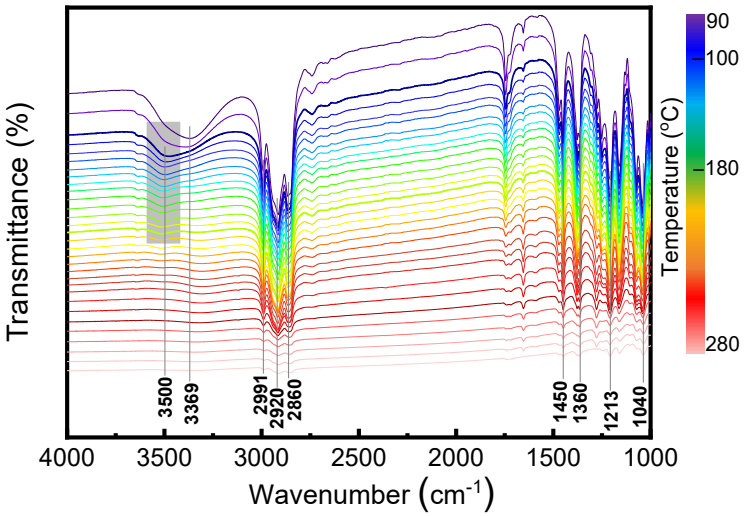

Fig. S2 Temperature-resolved FTIR spectra collected during the operando studies of PK3: at 90 °C, there is a broad band in the -OH area (at around 3400 cm^{-1}) due to absorbed water, and at 100 °C this peak shifts to 3500 cm^{-1} and becomes narrower, indicating the existence of terminal hydroxyl groups in PK3; the typical bands between 3000 and 2800 cm^{-1} correspond to the C-H stretching bands in alkanes, that at 1450 cm^{-1} is ascribed to the deformation vibration absorption of methylene, and that at 1040 cm^{-1} is attributed to the typical absorption band of ketal.[1]

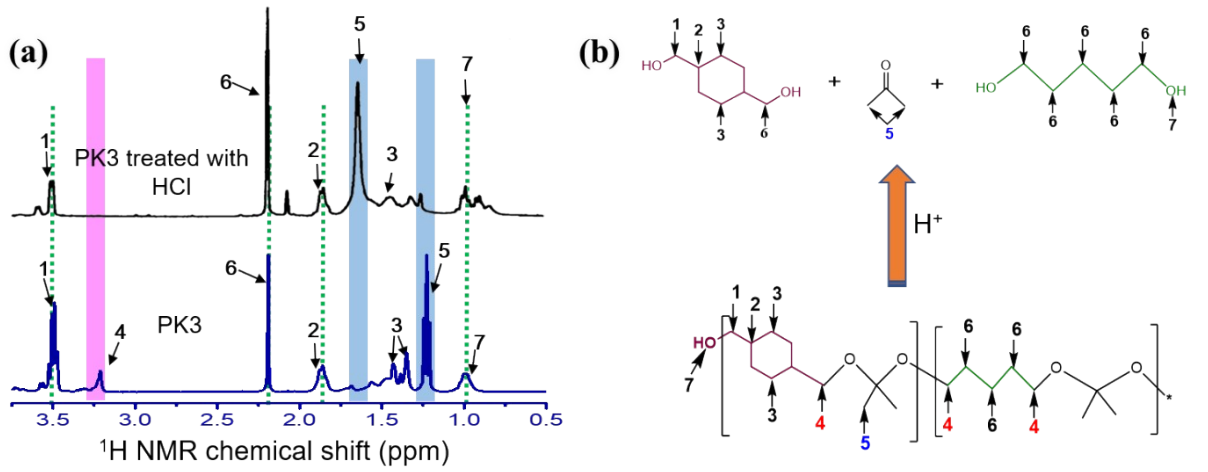

Fig. S3 Acid hydrolysis of PK3. (a) ^{1}H NMR spectra of PK3 before and after the acid solution treatment. In the spectrum of PK3 before the acid treated, the peaks at 3.48(**1**), 3.21(**4**) and 1.84(**2**) ppm are assigned to the methylene group directly attached to oxygen and the methyne group of cyclohexane, respectively, and those at 2.21(**6**) and 1.45(**3**) ppm correspond to the rest methylene groups in cyclohexane and 1,5-pentanediol, that at 1.25(**5**) ppm is assigned to the methyl originating from 2,2-dimethoxypropane, and that at 0.94(**7**) ppm is ascribed to the terminal alcohol.[2] The above results confirm the successful synthesis of PK3. After the acid treatment, the absence of the peak at **4** (marked with the pink rectangle) ascribed to methylene in contact with ketal indicates the hydrolysis of ketal, the emergence of the peaks at **5** at higher chemical shifts (marked by the blue rectangles) ascribed to methyl of acetone demonstrates the cleavage of PK3 into small molecules. (b) Schematic illustration of the acid hydrolysis of PK3 based on the results of the ^{1}H NMR characterization. Note: PK3 was composed of 78% 1,4-cyclohexanedimethanol and 22% 1,5-pentanediol, as calculated from the ^{1}H NMR spectrum of PK3 in Fig. S3a.

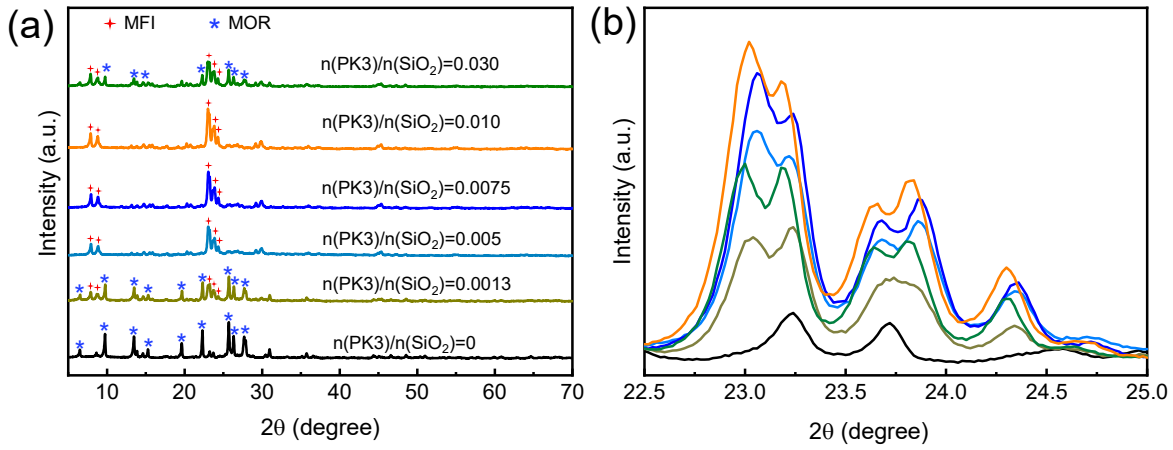

Fig. S4 XRD patterns of the samples synthesized with different amounts of PK3. (a) in the 2θ ranges of 5-70° and (b) 22.5-25°. Obviously, Na-$PK_{0.01}$-ZSM-5 has the strongest **peak intensity**.

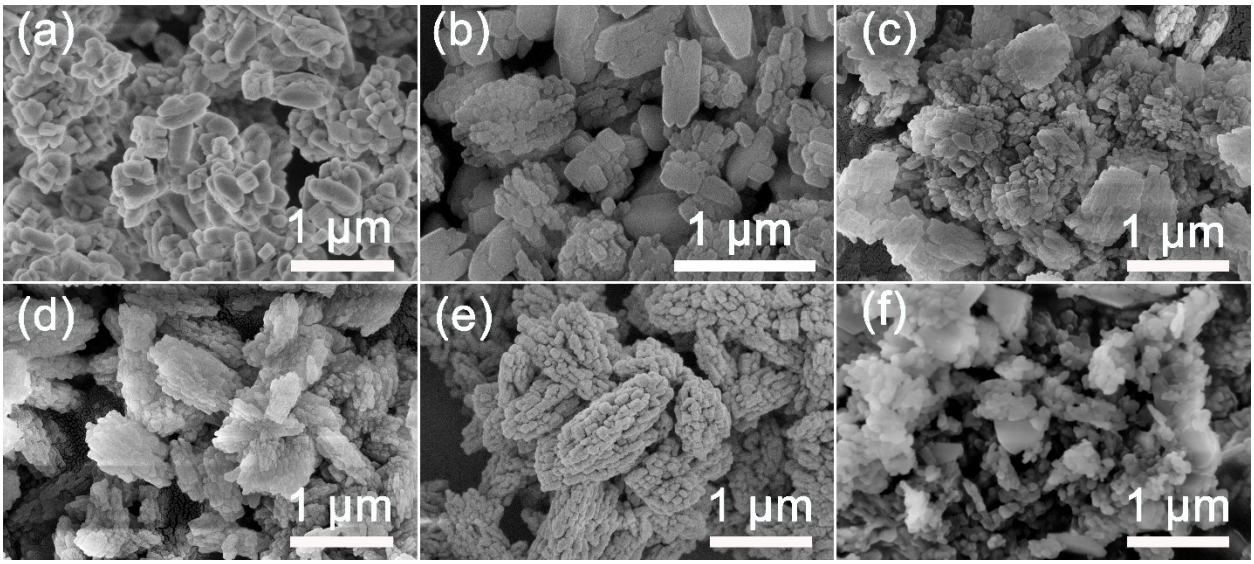

Fig. S5 SEM images of the samples synthesized with different amounts of PK3. (a) Na-PK_0-ZSM-5, (b) Na-$PK_{0.0013}$-ZSM-5, (c) Na-$PK_{0.005}$-ZSM-5, (d) Na-$PK_{0.0075}$-ZSM-5, (e) Na-$PK_{0.01}$-ZSM-5 and (f) Na-$PK_{0.03}$-ZSM-5.

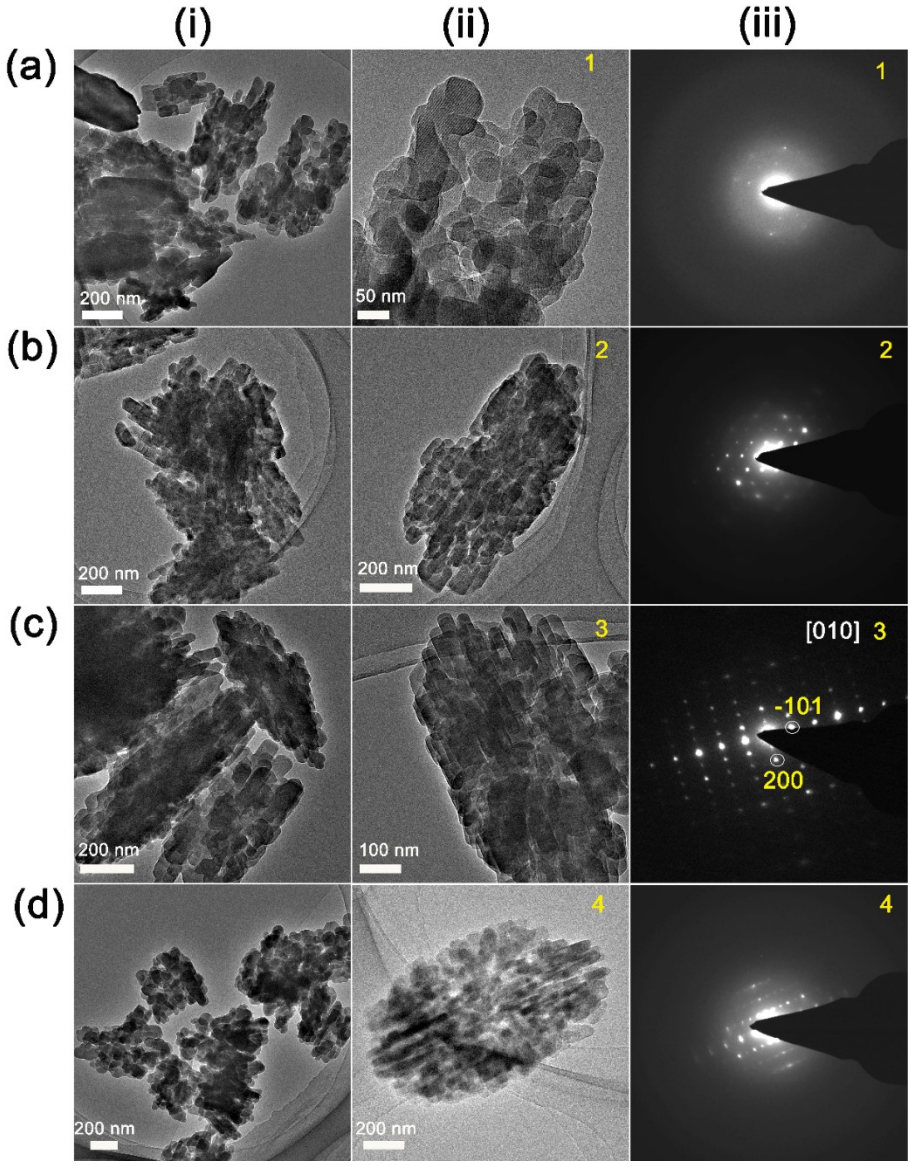

Fig. S6 TEM images of the samples synthesized with different amounts of PK3. (a) Na-$PK_{0.0013}$-ZSM-5, (b) Na-$PK_{0.005}$-ZSM-5, (c) Na-$PK_{0.01}$-ZSM-5 and (d) Na-$PK_{0.03}$-ZSM-5. (i) Low- and (ii) high- magnification TEM images of the products, and (iii) the corresponding SAED patterns taken from the entire particle of (ii).

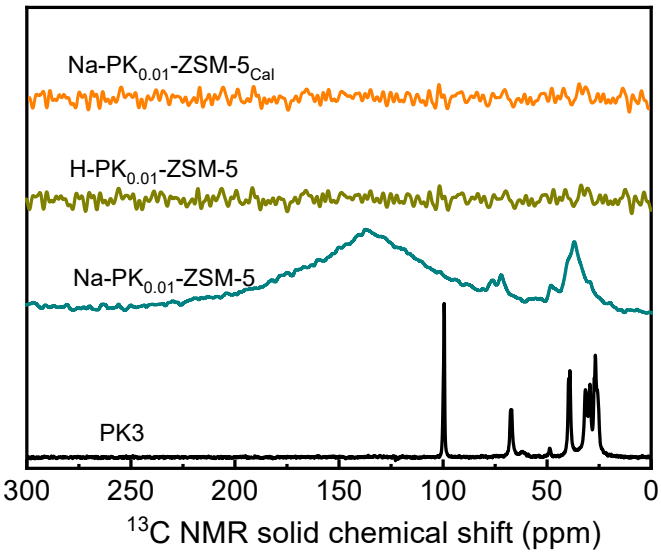

Fig. S7 Solid ^{13}C NMR spectra of PK3, Na-PK$_{0.01}$-ZSM-5, H-PK$_{0.01}$-ZSM-5 and Na-PK$_{0.01}$-ZSM-5$_{Cal}$.

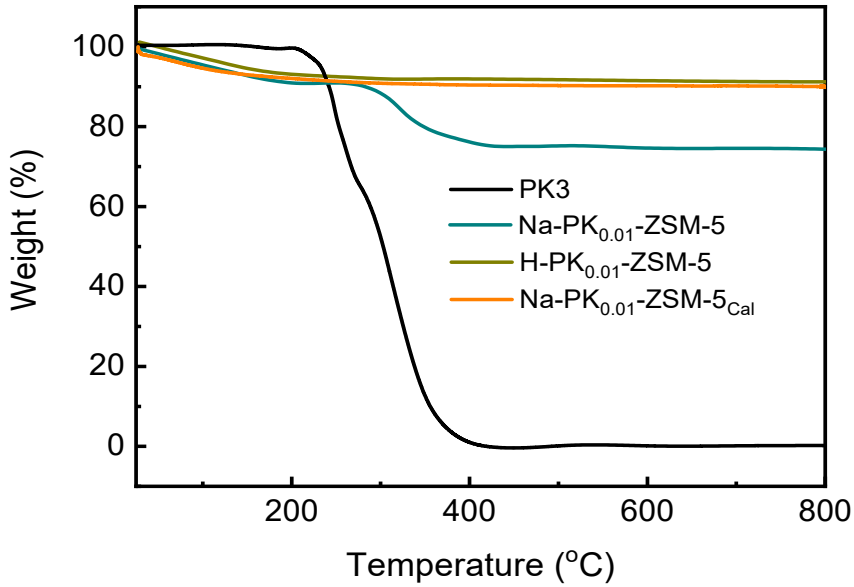

Fig. S8 TG curves of PK3, Na-$PK_{0.01}$-ZSM-5, H-$PK_{0.01}$-ZSM-5 and Na-$PK_{0.01}$-$ZSM\text{-}5_{Cal}$. The results show that Na-$PK_{0.01}$-ZSM-5 has a weight loss of ca. 10% below 200 °C due to the removal of physically absorbed water and a weight loss of ca. 15% in the temperature range of 200-430 °C. Apparently, the larger weight loss of Na-$PK_{0.01}$-ZSM-5 can be attributed to the removal of the template PK3. In contrast, Na-$PK_{0.01}$-$ZSM\text{-}5_{Cal}$ and H-$PK_{0.01}$-ZSM-5 exhibit weight losses of only ca. 1.90% and 1.70%, respectively, above 200 °C. These results demonstrate that PK3 can be removed from the zeolite framework through acid-exchange.

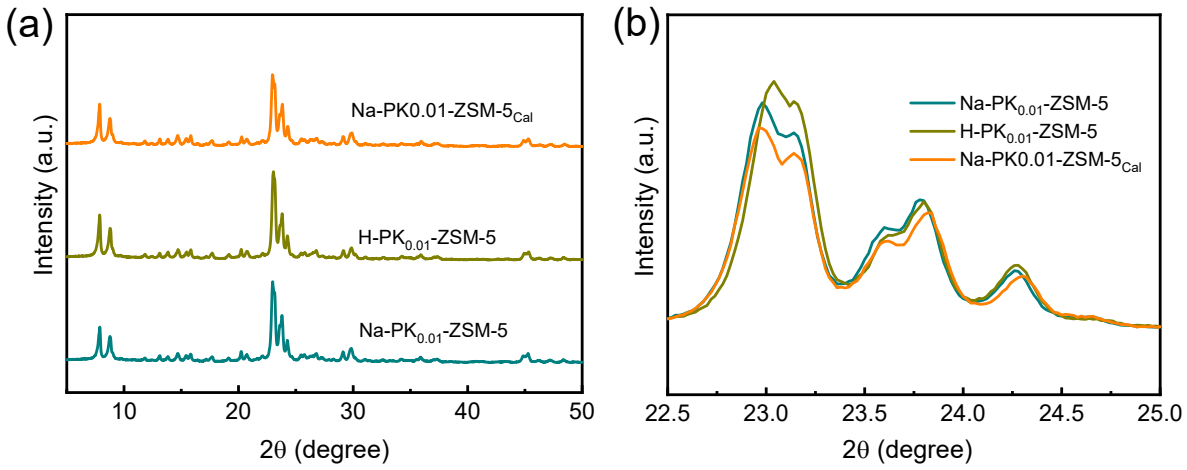

Fig. S9 XRD patterns of Na-PK$_{0.01}$-ZSM-5, H-PK$_{0.01}$-ZSM-5 and Na-PK$_{0.01}$-ZSM-5$_{Cal.}$ (a) in the 2θ ranges of 5-50° and (b) 22.5-25°. Obviously, H-PK$_{0.01}$-ZSM-5 has the strongest diffraction peaks. Compared with that (96%) of H-PK$_{0.01}$-ZSM-5, the crystallinity of Na-PK$_{0.01}$-ZSM-5$_{Cal}$ greatly drops to 90%, revealing the partial collapse of the zeolite framework after calcination. Interestingly, H-PK$_{0.01}$-ZSM-5 owns a higher crystallinity even outperforms its parent counterpart Na-PK$_{0.01}$-ZSM-5 (94%).

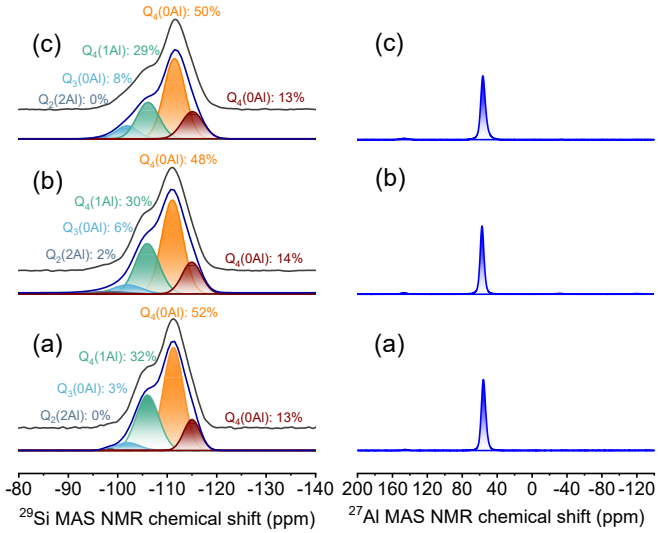

Fig. S10 ^{29}Si (left) and ^{27}Al (right) solid-state MAS NMR spectra of (a) Na-PK$_{0.01}$-ZSM-5, (b) Na-PK$_{0.01}$-ZSM-5$_{Cal}$ and (c) H-PK$_{0.01}$-ZSM-5. In the ^{29}Si MAS NMR spectra, the peaks at -98, -102 and -106 ppm correspond to Q^2(2Al), Q^3(0Al) and Q^4(1Al) Si species, respectively; and those at -112 and -115 ppm belong to Q^4(0Al) Si species. Framework n(SiO_2)/n(Al_2O_3) ratios (Table S2) were estimated from the peak areas of the different sites according to the known formula.[3] The simulation of the spectra gives n(SiO_2)/n(Al_2O_3) values of 25, 26, and 27 for Na-PK$_{0.01}$-ZSM-5, Na-PK$_{0.01}$-ZSM-5$_{Cal}$ and H-PK$_{0.01}$-ZSM-5, respectively. Additionally, the ^{27}Al MAS NMR spectra all exhibit the resonance located at 56 ppm corresponding to the tetrahedrally coordinated framework aluminum atoms with Brönsted acid sites.

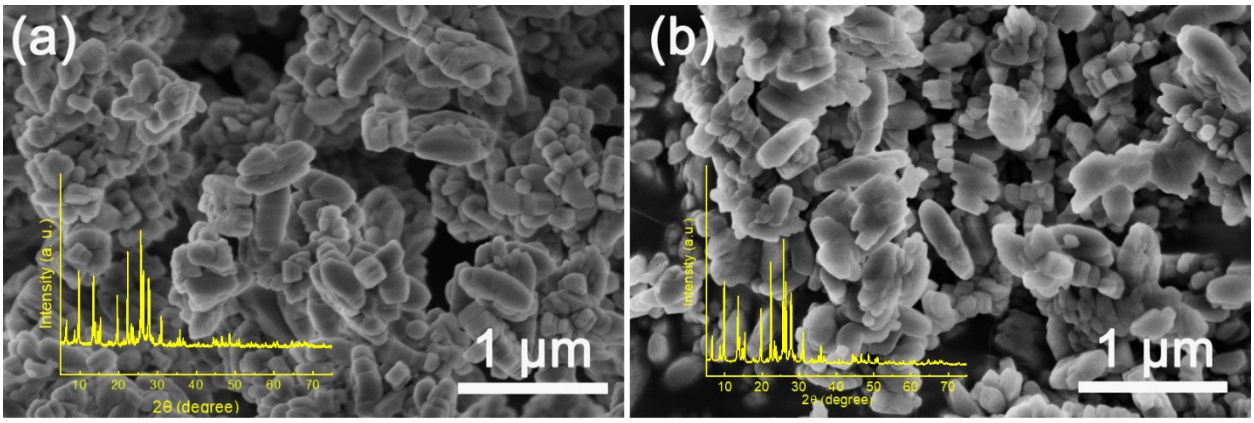

Fig. S11 (a) SEM images and XRD patterns (inset) of the sample obtained after crystallization for 80 and (b) 120 h in the absence of PK3.

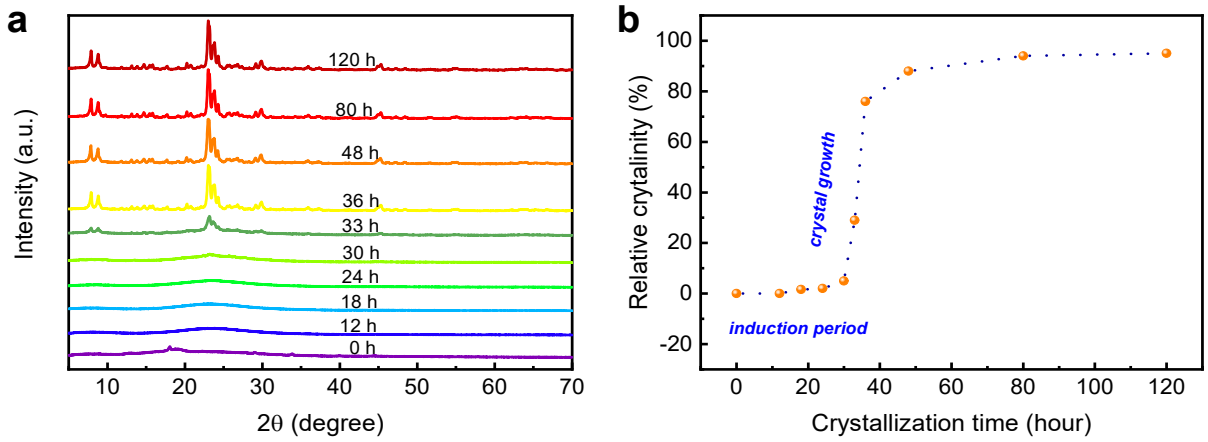

Fig. S12 Crystallization process of Na-PK$_{0.01}$-ZSM-5. (a) XRD patterns of the intermediates obtained after crystallization for different lengths of time at 160 °C and (b) the crystallization curve of Na-PK$_{0.01}$-ZSM-5. The first formation of zeolite crystals is obviously reflected by the XRD pattern of the intermediate obtained after crystallization for 33 h. Therefore, the first 30 h can be considered as the nucleation period.

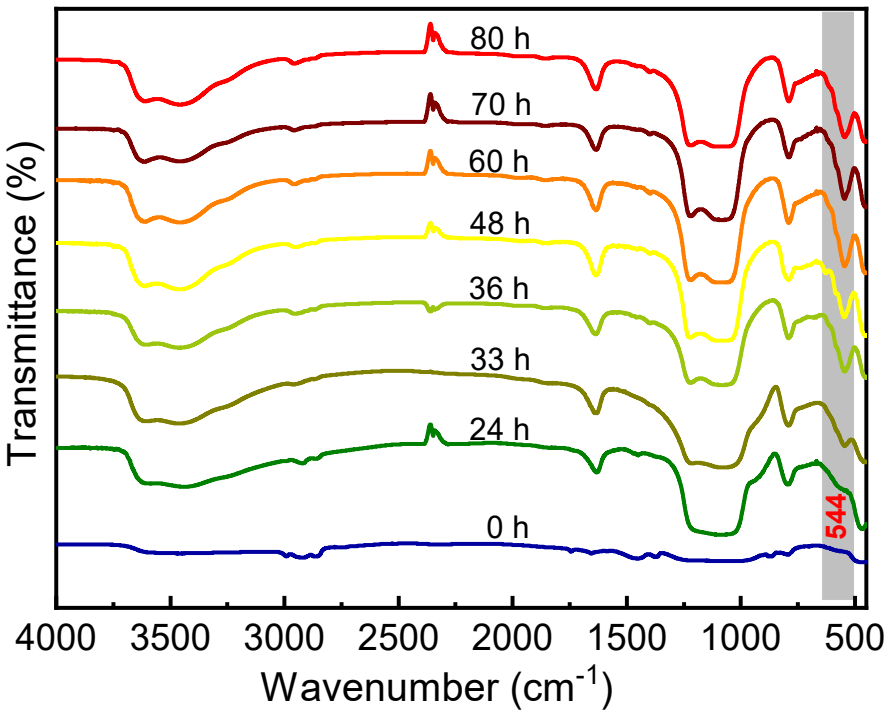

Fig. S13 FTIR spectra of the intermediates obtained after crystallization for different lengths of time at 160 °C with PK3 as the template. The peaks at 1080-1215 and 796 cm^{-1} are ascribed to the asymmetric and symmetric vibration modes of T-O-T (T = Si and Al) groups and the band at 544 cm^{-1} is attributed to the asymmetric stretching mode of the double 5-membered rings.[4]

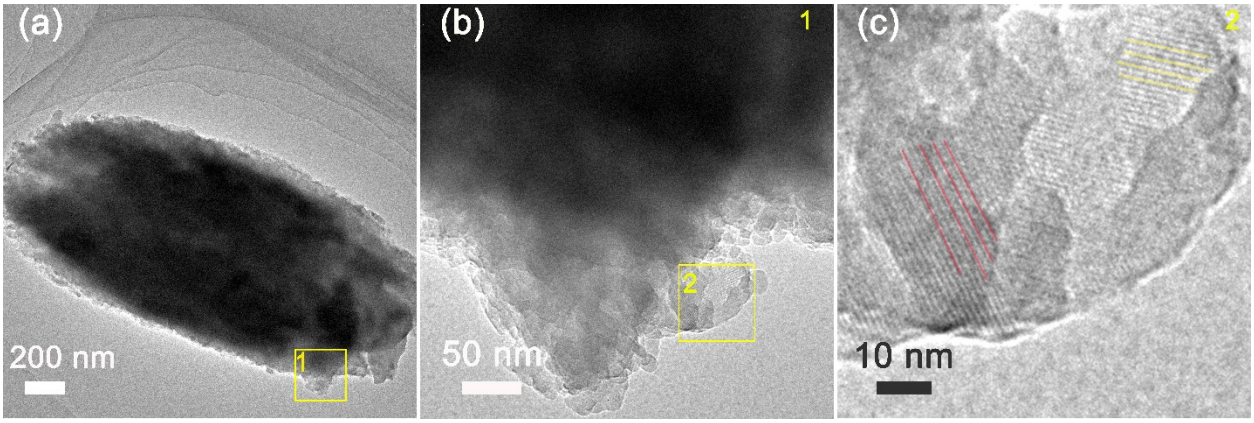

Fig. S14 TEM images of Na-PK$_{0.01}$-ZSM-5 (33 h). (a) Low magnification TEM image of Na-PK$_{0.01}$-ZSM-5 (33 h), (b) and (c) high-magnification TEM images from regions 1 and 2 marked in (a) and (b), respectively. The lines in (c) with different colors marking the lattice fringes show the different orientations.

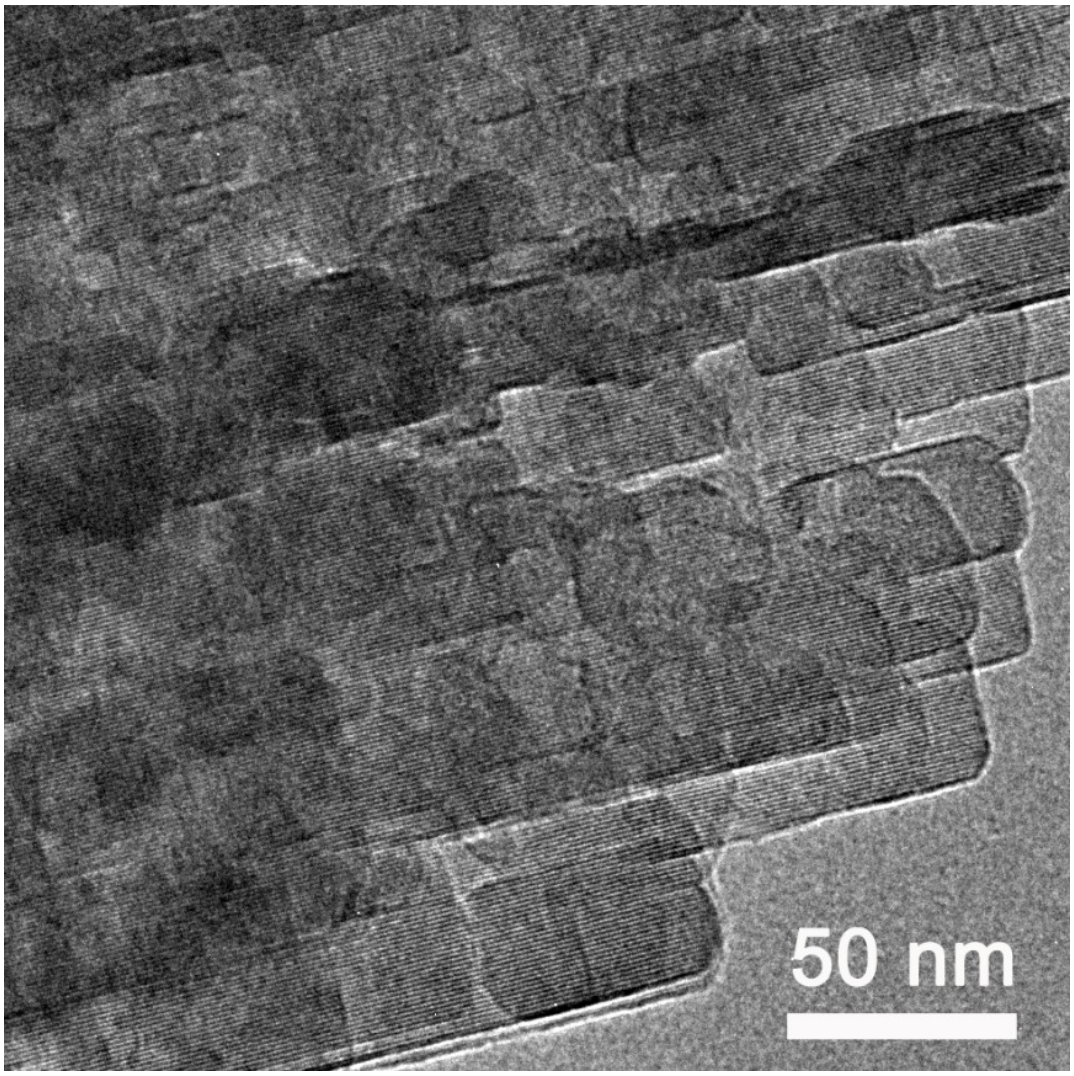

Fig. S15 High-magnification TEM image of Na-PK$_{0.01}$-ZSM-5 (36 h).

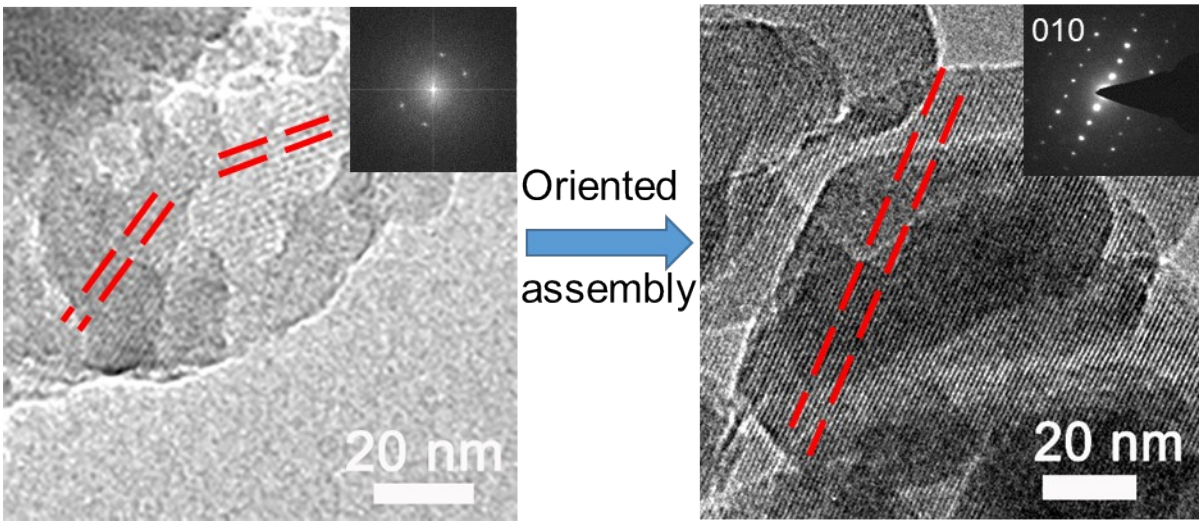

Fig. S16 Schematic of the oriented assembly of Na-PK$_{0.01}$-ZSM-5.

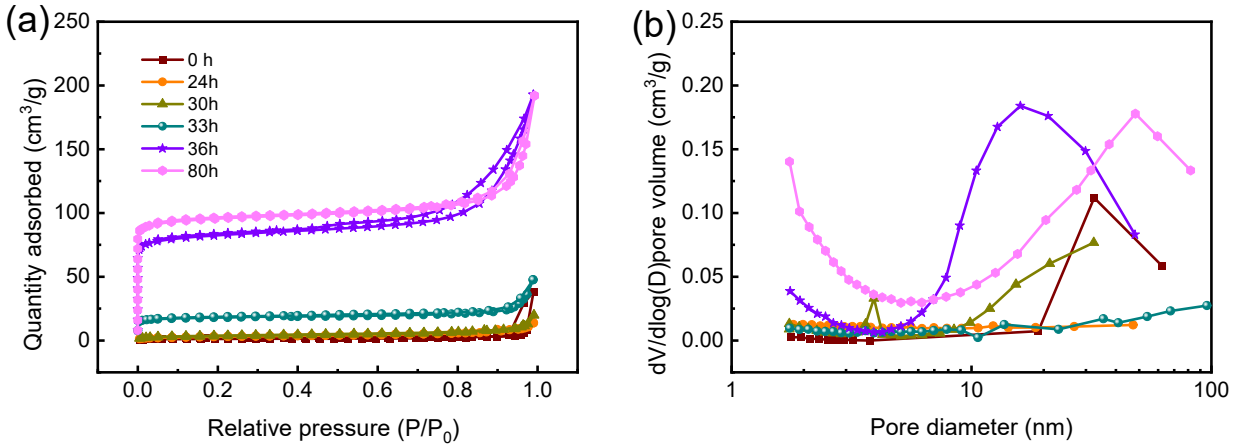

Fig. S17 Crystallization process of Na-PK$_{0.01}$-ZSM-5. (a) N_2 adsorption-desorption isotherms and (b) BJH pore size distribution curves of Na-PK$_{0.01}$-ZSM-5$_{Cal}$ (0 h), Na-PK$_{0.01}$-ZSM-5$_{Cal}$ (24 h), Na-PK$_{0.01}$-ZSM-5$_{Cal}$ (30 h), Na-PK$_{0.01}$-ZSM-5$_{Cal}$ (33 h), Na-PK$_{0.01}$-ZSM-5$_{Cal}$ (36 h) and Na-PK$_{0.01}$-ZSM-5$_{Cal}$ (80 h) crystallization at 160 ^{o}C.

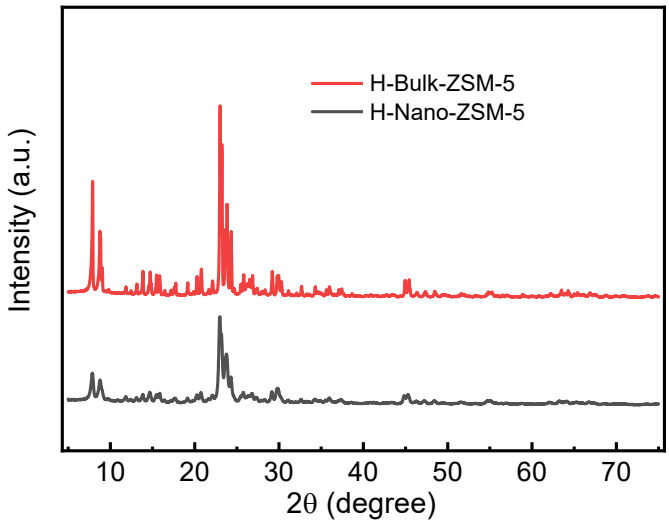

Fig. S18 XRD patterns of H-Bulk-ZSM-5 and H-Nano-ZSM-5.

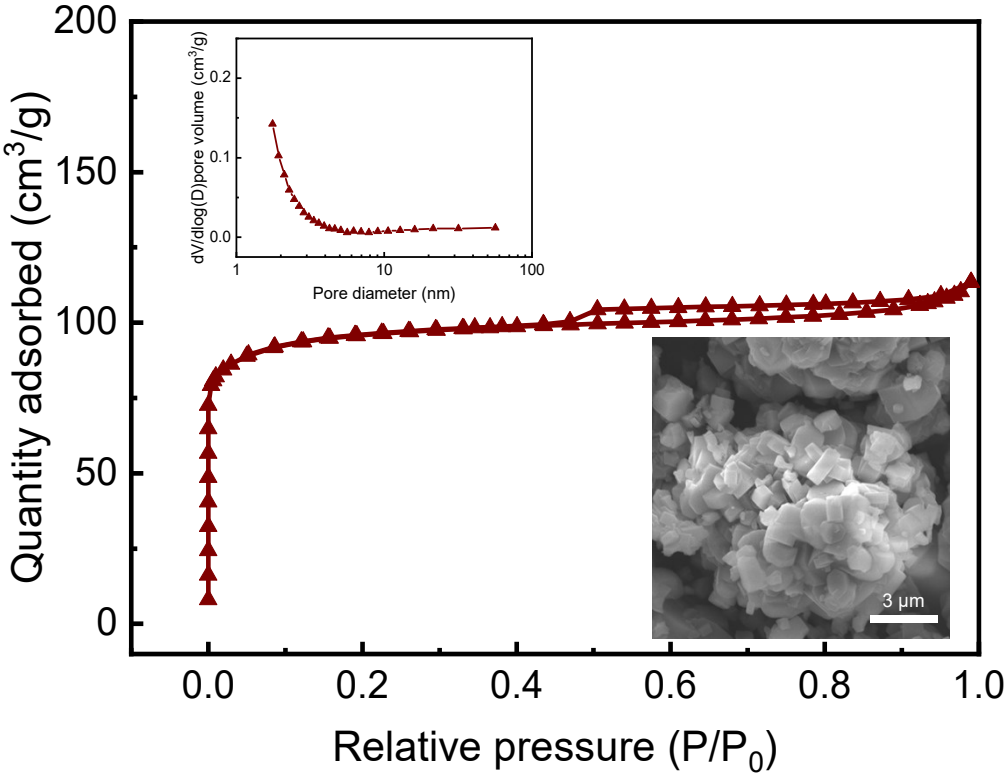

Fig. S19 N_2 adsorption-desorption isotherms, BJH pore size distribution curve (inset) and SEM image (inset) of H-Bulk-ZSM-5.

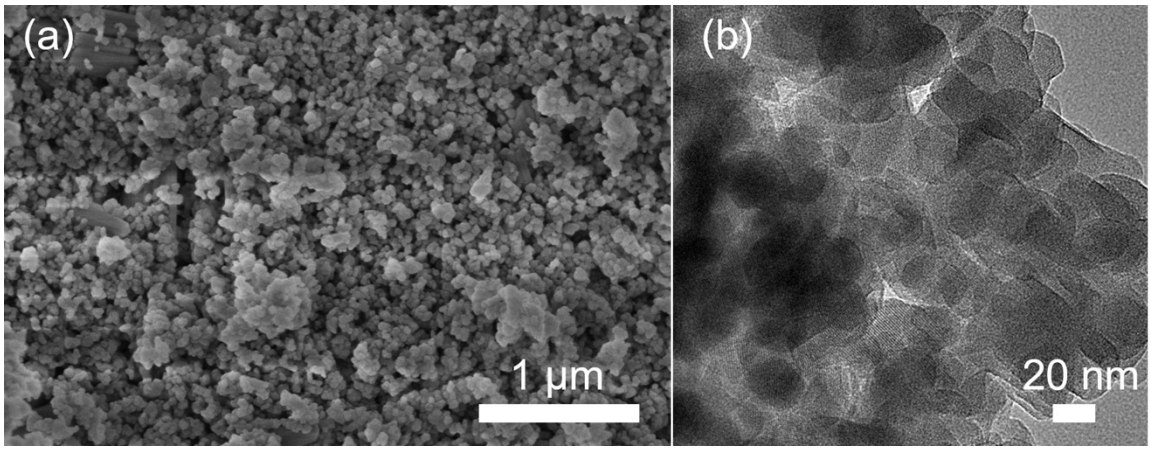

Fig. S20 Morphology of H-Nano-ZSM-5. (a) SEM and (b) TEM images of H-Nano-ZSM-5.

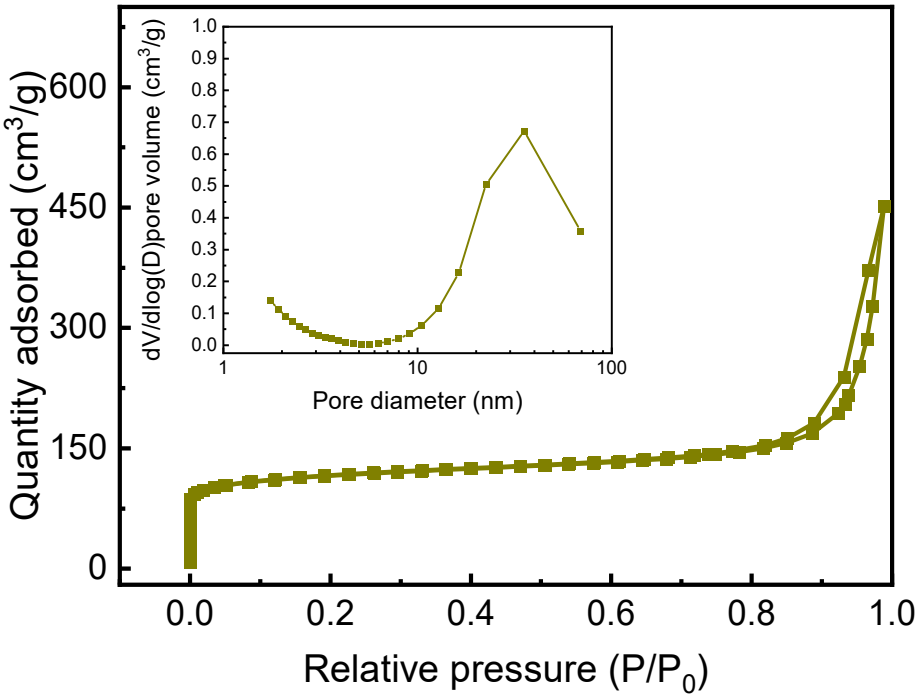

Fig. S21 N_2 adsorption-desorption isotherms and BJH pore size distribution curve (inset) of H-Nano-ZSM-5.

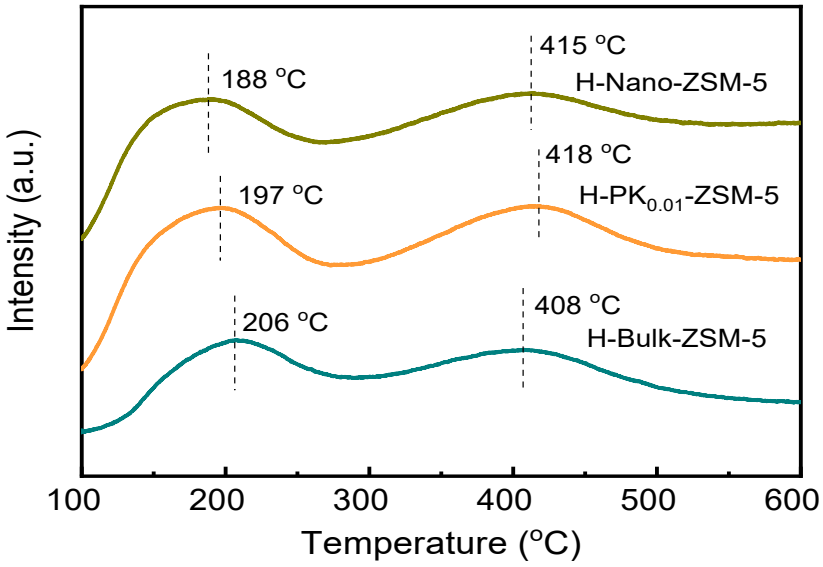

Fig. S22 NH_3-TPD profiles of H-Bulk-ZSM-5, H-Nano-ZSM-5 and H-$PK_{0.01}$-ZSM-5.

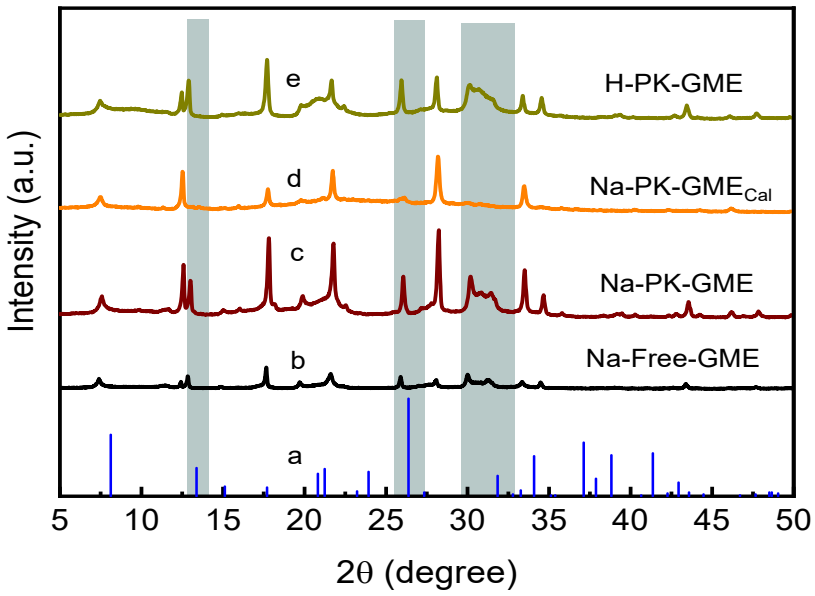

Fig. S23 Synthesis of GME. (a) Simulated pattern of the GME structure from PDF #38-0435, XRD patterns of (b) GME synthesized without the addition of the template (Na-Free-GME), (c) GME synthesized with PK3 as the template (Na-PK-GME), Na-PK-GME after (d) removing the template via calcination (Na-PK-GME$_{Cal}$) and (e) removing the template via acid-exchange (H-PK-GME). Compared with those of Na-Free-GME, the characteristic diffraction peaks of Na-PK-GME are stronger. It is obvious that the addition of PK3 promotes the crystallization of GME and increases the crystallinity. Clearly, after calcination at 550 °C to remove PK3, GME has been transformed into another phase; whereas, after the treatment with the citric acid solution, the structure of GME has not been destroyed. This indicates the applicability of the pH-smart polymer in synthesizing GME.

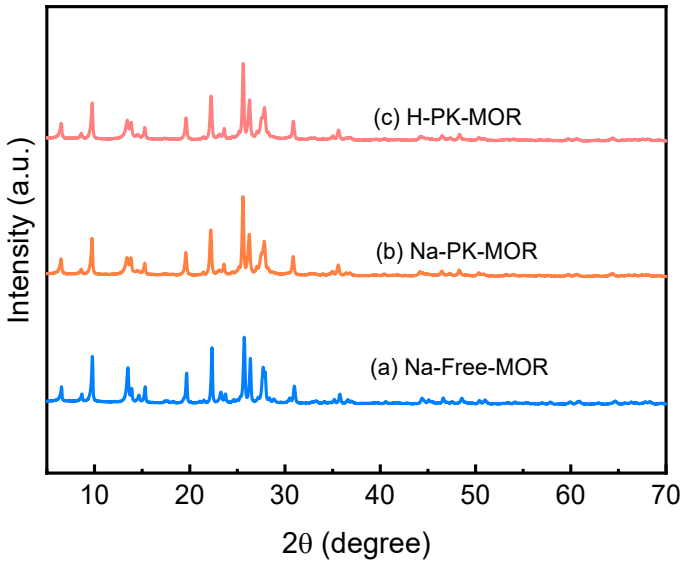

Fig. S24 Synthesis of MOR. XRD patterns of MOR synthesized (a) without the addition of the template (Na-Free-MOR), (b) with PK3 as the template (Na-PK-MOR), and (c) Na-PK-MOR after removing the template via acid-exchange (H-PK-MOR).

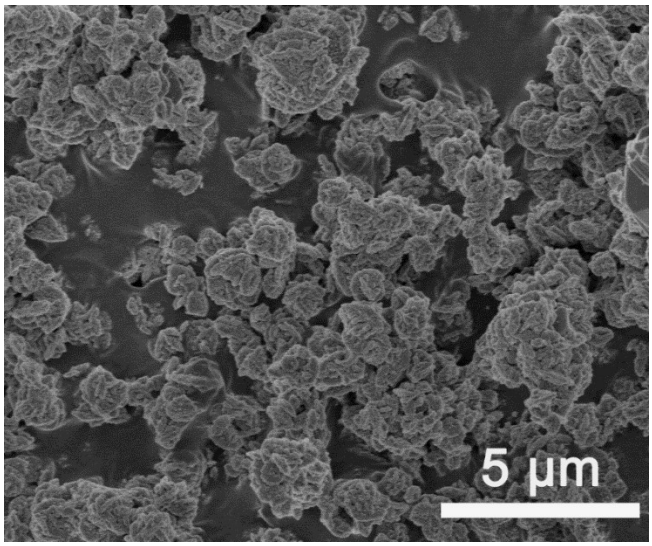

Fig. S25 SEM image of GME synthesized in the absence of PK3.

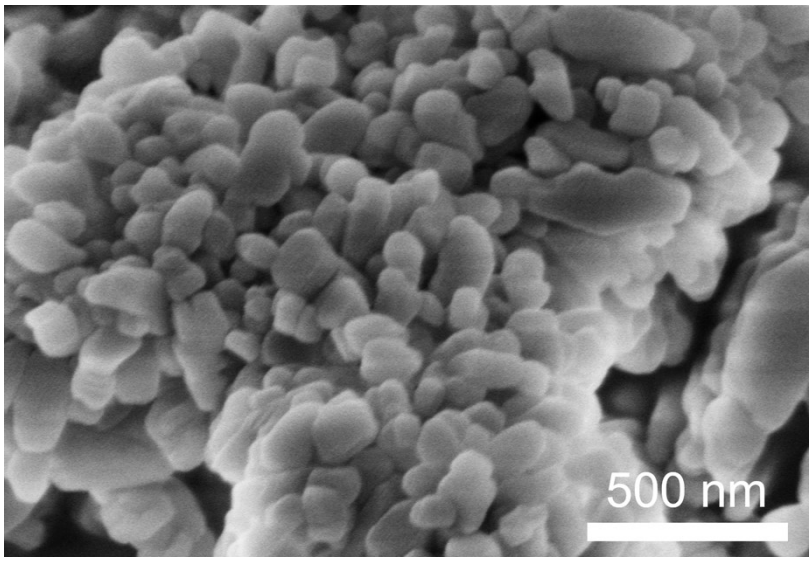

Fig. S26 SEM image of MOR synthesized in the absence of PK3.

Supplementary Tables

Table S1 Molecular weights of the synthesized ketal polymers determined by GPC

Sample	Adding times of DMP	M_n[a] (kDa)	M_w[b] (kDa)	PDI[c]
PK3-1	1	-[d]	-[d]	-[d]
PK3-2	3	0.70	1.30	1.86
PK3	5	3.00	3.90	1.30
PK3-4	8	3.30	4.80	1.45

Notes: [a]number-average molecular weight; [b]weight-average molecular weight; [c]polymer dispersity index; [d]indetectable by GPC.

Table S2 Characteristic properties of products synthesized with different amounts and molecular weights of PK3.

Item	Phase composition[a]	Relative crystallinity of ZSM-5 [a] (%)	S_{BET}[b] (m^2/g)	V_{meso}[c] (cm^3/g)
H-PK_0-ZSM-5	Mordenite	0	361	0.04
H-$PK_{0.0013}$-ZSM-5	Mordenite+ZSM-5	43	380	0.10
H-$PK_{0.005}$-ZSM-5	ZSM-5	77	398	0.12
H-$PK_{0.01}$-ZSM-5	ZSM-5	94	436	0.16
H-$PK_{0.03}$-ZSM-5	ZSM-5+Mordenite	66	360	0.10
H-PK3-$1_{0.01}$-ZSM-5	ZSM-5+Mordenite	76	290	0.10
H-PK3-$2_{0.01}$-ZSM-5	ZSM-5	93	421	0.15
H-PK3-$4_{0.01}$-ZSM-5	ZSM-5	88	340	0.17

Notes: [a]determined by XRD; [b]S_{BET} (total surface area) measured by Brunauer-Emmett-Teller (BET). [c]V_{meso} (mesopore volume) calculated using the t-plot method

Table S3 Chemical compositions of the different samples

Item	Atomic content (%)					$n(SiO_2)/n(Al_2O_3)$		
	Si[a]	Al[a]	O[a]	Na[a]	Na[b]	Bulk[a]	Bulk[b]	Framework[c]
Na-$PK_{0.01}$-ZSM-5	26.59	2.50	69.71	1.20	2.84	21	21	25
Na-$PK_{0.01}$-ZSM-5_{Cal}	25.54	2.44	70.82	1.20	2.75	21	21	26
H-$PK_{0.01}$-ZSM-5	26.66	2.13	71.21	0.00	0.02	25	25	27
H-Bulk-ZSM-5	23.99	1.89	74.11	0.01	-	25		-
H-Nano-ZSM-5	24.13	1.93	73.92	0.02	-	25		-

Notes: [a]measured by EDS; [b]measured by ICP; [c]calculated from the ^{29}Si MAS NMR spectra in Fig. S10.

Table S4 Textural parameters of Na-PK$_{0.01}$-ZSM-5 before and after removing the template

Sample	S_{BET}[a] (m^2/g)	S_{micro}[b] (m^2/g)	S_{meso}[b] (m^2/g)	V_{Total} (cm^3/g)	V_{micro}[b] (cm^3/g)	V_{meso}[b] (cm^3/g)
Na-PK$_{0.01}$-ZSM-5	10	0	10	0.049	0.000	0.049
H-PK$_{0.01}$-ZSM-5	436	306	130	0.32	0.16	0.16
Na-PK$_{0.01}$-ZSM-5$_{Cal}$	395	292	103	0.28	0.14	0.14

Notes: [a]total specific surface area calculated by applying the BET equation using the linear part ($0.05 < P/P_0 < 0.30$) of the adsorption isotherm; [b]micropore and mesopore specific surface areas, and micropore and mesopore volumes calculated by using the *t*-plot method, respectively.

Table S5 Textural parameters of the calcined Na-$PK_{0.01}$-ZSM-5 intermediates obtained after crystallization for different lengths of time

Sample	S_{BET}[a] (m^2/g)	S_{micro}[b] (m^2/g)	S_{meso}[b] (m^2/g)	V_{Total} (cm^3/g)	V_{micro}[b] (cm^3/g)	V_{meso}[b] (cm^3/g)
Na-$PK_{0.01}$-ZSM-5_{Cal} (0 h)	6	0	6	0.007	0.000	0.007
Na-$PK_{0.01}$-ZSM-5_{Cal} (24 h)	12.6	0.6	12	0.014	0.002	0.012
Na-$PK_{0.01}$-ZSM-5_{Cal} (30 h)	13	1	12	0.017	0.003	0.014
Na-$PK_{0.01}$-ZSM-5_{Cal} (33 h)	69	54	15	0.050	0.020	0.030
Na-$PK_{0.01}$-ZSM-5_{Cal} (36 h)	245	188	57	0.220	0.100	0.120
Na-$PK_{0.01}$-ZSM-5_{Cal} (48 h)	333	265	68	0.260	0.130	0.130
Na-$PK_{0.01}$-ZSM-5_{Cal} (80 h)	395	292	103	0.280	0.140	0.140

Notes: [a]total specific surface area calculated by applying the BET equation using the linear part ($0.05 < P/P_0 < 0.30$) of the adsorption isotherm; [b]micropore and mesopore specific surface areas, and micropore and mesopore volumes calculated by using the *t*-plot method, respectively.

Table S6 Textural parameters of the different samples

Sample	S_{BET}[a] (m^2/g)	S_{micro}[b] (m^2/g)	S_{meso}[b] (m^2/g)	V_{Total} (cm^3/g)	V_{micro}[b] (cm^3/g)	V_{meso}[b] (cm^3/g)
H-Nano-ZSM-5	390	268	122	0.31	0.14	0.17
H-Bulk-ZSM-5	323	249	74	0.17	0.13	0.04
H-PK-MOR	527	462	65	0.26	0.16	0.10
H-PK-GME	388	316	72	0.24	0.14	0.10

Notes: [a]total specific surface area calculated by applying the BET equation using the linear part ($0.05 < P/P_0 < 0.30$) of the adsorption isotherm; [b] micropore and mesopore specific surface areas, and micropore and mesopore volumes calculated using the *t*-plot method, respectively.

Table S7 Acid sites and peak areas of H-Bulk-ZSM-5, H-PK$_{0.01}$-ZSM-5 and H-Nano-ZSM-5.

Sample	T_M[a] (°C)		Total area	Peak area[b] (a.u.)	
	I	II	(a.u.)	I	II
H-Bulk-ZSM-5	206	408	6.7	2.5	4.2
H-PK$_{0.01}$-ZSM-5	197	418	15.3	5.3	10.0
H-Nano-ZSM-5	188	415	14.2	4.3	9.9

Notes: [a]center temperature of the peaks representing the different acid sites; [b]calculated from the peak areas of the different acid sites from the NH_3-TPD profiles in Fig. S22.

Supplementary References

1. Y. Wang, B. Chang and W. Yang, *J. Nanosci. Nanotechno.,* 2012, **12**, 8266-8275.
2. S. C. Yang, M. Bhide, I. N. Crispe, R. H. Pierce and N. Murthy, *Bioconjugate Chem.,* 2008, **19**, 1164-1169.
3. X. Zhu, L. Wu, P. C. M. M. Magusin, B. Mezari and E. J. M. Hensen, *J. Catal.,* 2015, **327**, 10-21.
4. B. Zhang, M. Douthwaite, Q. Liu, C. Zhang, Q. Wu, R. Shi, P. Wu, K. Liu, Z. Wang, W. Lin, H. Cheng, D. Ma, F. Zhao and G. J. Hutchings, *Green Chem.,* 2020, **22**, 1630-1638.